# All chemical $YBa_2Cu_3O_7$ superconducting multilayers: Critical role of $CeO_2$ cap layer flatness

M. Coll[a] and J. Gàzquez
*Institut de Ciencia de Materials de Barcelona–Consejo Superior de Investigaciones Cientificas (ICMAB/CSIC) Campus de la UAB, Barcelona 08193, Spain*

R. Hühne and B. Holzapfel
*Leibniz Institute for Solid State and Materials Research Dresden (IFW Dresden), Institute for Metallic Materials, 01171 Dresden, Germany*

Y. Morilla and J. García-López
*Centro Nacional de Aceleradores, E-41092 Sevilla, Spain*

A. Pomar, F. Sandiumenge, T. Puig, and X. Obradors[b]
*Institut de Ciencia de Materials de Barcelona–Consejo Superior de Investigaciones Cientificas (ICMAB/CSIC) Campus de la UAB, Barcelona 08193, Spain*

(Received 30 June 2008; accepted 8 December 2008)

New advances toward microstructural improvement of epitaxial $CeO_2$ films grown by chemical solution deposition and their use as buffer layers for $YBa_2Cu_3O_7$ (YBCO) films are presented. We demonstrate that the degree of epitaxy and the fraction of (001) atomically flat surface area are controlled by the incorporation of tetravalent ($Zr^{4+}$) or trivalent ($Gd^{3+}$) cations into the ceria lattice. The degree of epitaxy has been investigated by means of Rutherford backscattering spectroscopy-channeling and reflection high-energy electron diffraction. In addition, we use a new methodology to quantify the fraction of (001) atomically flat area from atomic force microscopy images. Results are further correlated with the superconducting properties, microstructure, and texture of YBCO films grown by the trifluoroacetate route. A comparison with pulsed laser deposition and YBCO films grown on the same ceria layers is also presented. This growth procedure has allowed us to obtain all chemical multilayer films with controlled microstructure and critical current densities above 4 MA $cm^{-2}$ at 77 K.

## I. INTRODUCTION

The production of affordable $YBa_2Cu_3O_7$ (YBCO) coated conductors (CC) is an extremely challenging issue for electric power applications.[1,2] Great effort is being devoted to finding simple multilayer architectures, which simultaneously satisfy an effective oxidation protection for the metallic substrate, an effective chemical barrier to cation diffusion, and a good lattice matching with a substrate and superconducting layer. Physical vapor deposition (PVD) techniques can certainly produce high-quality YBCO CC using numerous oxide buffer architectures where $J_c$ values of several MA $cm^{-2}$ at 77 K are routinely achieved.[3–5] However, the major goal now for CC technology to be competitive is to demonstrate the suitability of low-cost deposition techniques, such as chemical solution deposition (CSD) in which YBCO is grown by the trifluoroacetate route (TFA)[6,7] and buffer layers by metalorganic decomposition (MOD).[8–10] MOD- $SrTiO_3$ and MOD- $CeO_2$ have capitalized the attention of the researchers for its high potential as cap layers. Indeed, attractive $J_c$ values [$\sim$1 MA/$cm^2$ (77 K)] have been obtained using MOD-(Nb-doped) $SrTiO_3$ as single buffer layer on Ni-rolling-assisted biaxially textured substrates (RABiTs),[11] MOD-$CeO_2$ on MOD-$La_2Zr_2O_7$ buffered Ni-RABITs,[12] or MOD-$CeO_2$ on ion-beam-assisted deposition (IBAD)-stainless steel[13]; however, they are far from the target value of 3–4 MA/$cm^2$ at 77 K. So far the great potential of $CeO_2$ on Ni-RABiT has been limited to medium low-cost approaches[10,14–16] mostly because of the complexity to obtain highly textured MOD-$CeO_2$ under reducing atmosphere to match the criteria protection of the metallic substrate. Detailed studies on the growth mechanism and microstructure evolution of nanostructured MOD-$CeO_2$ on (001)YSZ single-crystal substrates revealed that under reducing atmospheres, carbon impurities from metal organic precursors decorate grain boundaries inhibiting the epitaxial grain growth.[17] More recently this main drawback has been overcome by modifying

Address all correspondence to these authors.
[a]e-mail: mcollbau@nist.gov
[b]e-mail: obradors@icmab.es
DOI: 10.1557/JMR.2009.0160

 

the kinetics of $CeO_2$ growth by the incorporation of dopant agents[18,19] or by using nitrate-based ceria precursor.[20] However, the fabrication of all-chemical YBCO multilayered structure based on $CeO_2$ cap layer remains the largest challenge.

It is known that the properties of buffer layers can dramatically affect the final properties of the YBCO film. Most of the studies have focused on improving in-plane texture of both YBCO and buffer layers; however, to approach this issue it is also important to have a tight control of the interface quality. It was recently demonstrated that it requires a fine control of the surface morphology of the cap layer,[21–23] in particular, it is necessary to consider the percentage of flat area beyond the traditional root mean square (rms) roughness.[24] This parameter can be controlled by postannealing treatments, processing atmosphere, temperature, or chemical composition, depending on the nature of the oxide buffer.[23,25] The next step to obtain high quality all-chemical YBCO-$CeO_2$-based multilayer is to fully understand the influence of MOD-$CeO_2$ surface quality on the microstructure and critical current densities of YBCO film.

The main goal of this work is to assess the role of the surface flatness of MOD-$CeO_2$ films on YBCO critical current densities grown by two different routes: TFA and pulsed laser deposition (PLD). In Sec. III. A we report a systematic study of the influence of composition (doping by $Zr^{4+}$ or $Gd^{3+}$), and processing atmosphere on the MOD-$CeO_2$ properties, focusing on the surface quality. Then, in Sec. III. B we analyze the influence of the surface quality of the doped $CeO_2$ layers on the TFA- and PLD-YBCO films microstructure and critical current densities. For all-chemical multilayer structures we have proved that highly crystalline and atomically flat $CeO_2$ surfaces (>70%) promote epitaxial TFA-YBCO films with critical current densities above 4 MA/cm$^2$. These optimal surfaces can be achieved, both by the incorporation of dopants, such as $Gd^{3+}$ and $Zr^{4+}$, or under oxidizing atmospheres. For PLD-YBCO films grown on MOD-$CeO_2$ cap layers, a less restrictive situation has been observed where good quality multilayers can already be achieved on $CeO_2$ films with a flatness of about 30%.

## II. EXPERIMENTAL DETAILS

Precursor solutions were prepared by dissolution of stoichiometric amounts of gadolinium acetylacetonate [$Gd(CH_3COCHCOCH_3)_3$, 99.9% from Aldrich, Milwaukee, WI] or zirconium acetylacetonate [$Zr(CH_3COCHCOCH_3)_3$] (Aldrich), in 1 mL of propionic acid (Aldrich) and 1 mL of anhydrous isopropanol (Aldrich). The solution was stirred and heated to 40 °C for 20 min, followed by the incorporation of cerium (III) acetylacetonate hydrate [$Ce(CH_3COCHCOCH_3)_3 \times H_2O$, 99.9%, Alfa Aesar, Ward Hill, MA], and then stirred for another 20 min at 60 °C obtaining a yellow and transparent solution. Ten percent of dopant concentration was used throughout this work and the total metal ion concentration was adjusted to 0.25 M. The final precursor solution was kept in sealed vials for several months. The solution lifetime was controlled by measuring its viscosity at room temperature (3 MPas) using a rheometer.

$CeO_2$ films were grown by depositing 15 μL of the precursor solution onto 5 mm × 5 mm (001)-cut Y-stabilized $ZrO_2$ (YSZ) single-crystal substrates, previously cleaned for 10 min in acetone and 10 min in methanol using an ultrasonic bath. Deposition was performed with a rotation speed of 6000 rpm, rotation time of 2 min, and an acceleration of 3000 rpm s$^{-1}$. After spin-coating, samples were heated in a tubular furnace at 1500 °C/h up to 700–900 °C, then held for 8 h to allow completion on the epitaxial transformation of the precursor, and finally cooled to room temperature. Film growth was carried out under Ar/5%$H_2$ or $O_2$ atmosphere. These deposition and growth conditions yielded films with a final thickness of ~30 nm.

The preparation of YBCO films were carried out by two different techniques. With the first technique, YBCO films were prepared from an anhydrous trifluoroacetate solution, details about this preparation can be found elsewhere.[26] The concentration of TFA solutions used in this work was 1.5 M and the film thicknesses investigated were in the range 200–250 nm. The pyrolysis process that followed after the solution deposition process was performed with a fast thermal profile lasting for 2 h, which has been described in detail in Ref. 27. After pyrolysis, a high temperature annealing was performed at 750 °C under a wet nitrogen atmosphere with $PH_2O$ = 40 mbar and $PO_2$ = 0.2 mbar for 3 h. Finally, a standard oxygenation process was performed at 450 °C for 3 h. All these parameters have been optimized for the growth on MOD-$CeO_2$ cap layer based on a previously reported study of TFA-YBCO growth on single-crystal substrate.[28]

With the second technique, high quality 300-nm-thick YBCO films were prepared by PLD in standard geometry using a KrF-excimer (Lambda Physik LPX305i, Göttingen, Germany) laser running at 5 Hz with a deposition rate of about 1 Å/pulse. The deposition was carried out in an oxygen atmosphere, $PO_2$ = 0.3 mbar with a substrate temperature of 810 °C. After deposition the samples were cooled in 400 mbar $O_2$.[29]

Structural properties and surface morphology of the films were investigated by Rutherford backscattering/channeling (RBS/C), x-ray diffraction (XRD), reflection high-energy electron diffraction (RHEED), and atomic force microscopy (AFM). RBS/C measurements[30] were performed to determine the crystal quality and degree of epitaxy of $CeO_2$ layers using a 2 MeV $He^+$ beam. The backscattered particles were detected at 165° with

respect to the beam direction. AFM images were measured in tapping mode. The images were processed with the software package WSxM from Nanotec Electronica S.L. (http://www.nanotec.es)[31] and PicoScan Version 5.3.3 Molecular Imaging. XRD measurements were carried out using Bruker-AXS GADDS (Berlin, Germany). This system is equipped with a two-dimensional (2D) XRD detector and allows the examination of a wide range of reciprocal space and allows us to easily infer the coexistence of textured and randomly oriented crystallographic phases. A wide range of materials, including thin films and powder, have successfully been analyzed by this instrument.[32,33] RHEED patterns were obtained with a Staib Instruments system (Germany) using an electron beam of 30 kV, a beam current of about 50 μA, and an incidence angle of less than 2° with respect to the substrate surface. The incidence directions were parallel to the ⟨100⟩ of the YSZ. The microstructure and local chemical composition of the samples were characterized by cross-sectional low magnification and high-resolution transmission electron microscopy (TEM and HRTEM) using a JEOL 2010 FEG electron microscope (Tokyo, Japan) operated at 200 kV (point-to-point resolution 0.19 nm) equipped with a Gatan Image Filter 2000 EELS spectrometer with an energy resolution of 0.8 eV. Thin foils for TEM observation were prepared by the conventional cutting, gluing, and grinding procedures, followed by a final milling step with Ar ions down to perforation.

Critical current density ($J_c$) of our YBCO films was measured with a Quantum Design SQUID magnetometer (San Diego, CA) provided with a 5.5 T and 7 T superconducting coils. The $J_c$ was determined inductively from hysteretic magnetization measurements based on the critical state model as applied to thin films.[34]

## III. RESULTS AND DISCUSSION

### A. MOD-$CeO_2$ films

We describe four $CeO_2$ films with different surface morphology purposely modified: pure $CeO_2$, Gd-doped $CeO_2$ (noted CGO), Zr-doped $CeO_2$ (noted CZO) all of them grown under reducing atmospheres, and Zr-doped $CeO_2$ film grown under oxygen atmosphere (noted CZO $O_2$). All of these samples were prepared using the same deposition parameters and heating profile.

RBS in random and channeling geometries were performed to quantitatively measure the crystal perfection of these sets of samples. When a sample is channeled, the rows of atoms in the lattice are aligned parallel to the incident He ion beam. When imperfections or impurities in the lattice exist, backscattering signal will increase. By measuring the reduction in the backscattering signal when a sample is aligned along a preferred direction from a nonaligned sample it is possible to quantitatively measure the crystal perfection of a sample. The ratio between the yield for aligned and random directions is named $\chi_{min}$. In our experimental conditions, the $\chi_{min}$ for YSZ single-crystal substrate aligned along the ⟨100⟩ axis is ~7%.

RBS random and the ⟨100⟩ channeled spectra for YSZ single crystal (reference spectrum) and $CeO_2$, CGO, CZO, and CZO $O_2$ samples are shown in Figs. 1(a)–1(e), respectively. Arrows indicate the energetic positions for backscattering from Zr(Y) and Ce(Gd) atoms at the surface. Note that mass resolution is not enough to separate the Zr–Y and Ce–Gd signals. The $\chi_{min}$ for Ce atoms leads to 46% for the pure film, 24% and 22% for CGO and CZO films, respectively, and in the case of CZO $O_2$ $\chi_{min}$ was 12%. Accordingly, $CeO_2$ crystalline quality appears to improve with the incorporation of a dopant obtaining better crystallinity in oxygen atmosphere.

Figures 2(a)–2(d) show a series of 2 μm × 2 μm AFM topographic images for each $CeO_2$ sample. First, undoped $CeO_2$ film [Fig. 2(a)] presented a surface morphology dictated by rounded grains. By the incorporation of dopant agents, $Zr^{4+}$ or $Gd^{3+}$, round-shaped grains transform into terraces, and are larger in the case of trivalent cation [Figs. 2(b) and 2(c), respectively]. Finally, oxygen atmosphere further enhances the development of large terraces [Fig. 2(d)]. This morphological evolution is better appreciated if we carefully inspect the typical height profiles presented below the topographic images in Fig. 2. It is easily seen that modified $CeO_2$ films display flat terraces with sizes ranging from 100 nm in the case of CZO under reducing conditions to 400 nm for the sample processed under oxygen atmosphere. Surface roughness has also been calculated for each film using the typical statistical parameter rms (pure $CeO_2$ is 3.2 nm, CZO is 4.1 nm, CGO is 4.3 nm, and CZO $O_2$ is 1.5 nm). However, the surface quality of CSD multilayers cannot be simply described by this statistical parameter, as we will show later, it is required to characterize strictly the local quality of the buffer layer surface morphology, i.e., the atomically flat area. Thus, we propose a new type of analysis that estimates the percentage of atomically flat surface.[24] Our analysis shows that we can use the value of 1.5 nm as threshold value for flat area (3 unit cells of $CeO_2$) and then apply a binary operator to the AFM topographic images. This operator computes the area comprised within this height window resulting the binary images shown in the bottom of Figs. 2(a)–2(d) where the blue area corresponds to atomically flat grains. The proposed image analysis allows us to determine the percentage of atomically flat area for this series of $CeO_2$ samples, indicated in the corresponding figures. It is observed that the flat area increases from ~18% (pure $CeO_2$ film) to 30% (CZO), 71% (CGO), and 93% (CZO $O_2$). This type of surface

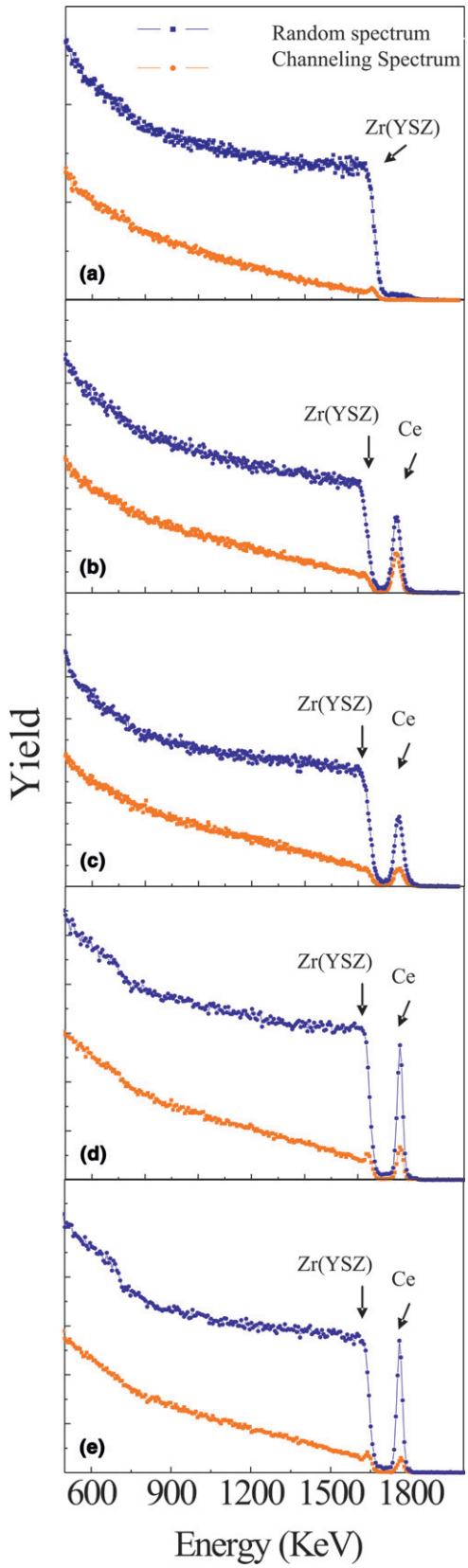


FIG. 1. Channeling and random RBS spectra along the ⟨001⟩ axis of the sample (a) YSZ single crystal, (b) $CeO_2$/YSZ, (c) CGO/YSZ, (d) CZO/YSZ, and (e) CZO ($O_2$)/YSZ. (color online)

analysis has been successfully carried out in other oxide buffer layers, i.e., $La_{0.7}Sr_{0.3}MnO_3$ solution derived buffer layers[22] and $CeO_2$ PVD layers.[35] Hence, it has proved useful to evaluate surface quality for multilayer growth.

Moreover, RHEED images were recorded in the ⟨001⟩ substrate direction for all samples to obtain an average measure of surface disorder (Fig. 3). Undoped $CeO_2$ film [Fig. 3(a)] shows diffraction rings in the RHEED pattern revealing a randomly oriented crystalline surface as a result of grain growth inhibition mechanism induced by C trapped at grain boundaries.[17] An important result, in view of the application of such films as buffer layers, is that the surface disorder is suppressed by the incorporation of dopant agents ($Zr^{4+}$ and $Gd^{3+}$) or using oxidizing atmospheres, as indicated by the ordered array of spots appearing in the RHEED pattern [Figs. 3(b)–3(d), respectively] and in good agreement with RBS/C results (Fig. 1). From these (001) textured films we can also detect an evolution from spotty to streaklike RHEED diffraction patterns reflecting an evolution from three-dimensional (3D) to 2D surface morphology in good agreement with our AFM analysis. Therefore, transformation of partially textured $CeO_2$ film into an epitaxial one can be achieved under oxygen atmosphere, as previously suggested by Cavallaro et al.[17] in pure $CeO_2$ samples or even under $Ar/H_2$ atmosphere by the incorporation of dopant agents.[18] It is noteworthy that the former conditions lead to a feasible cap layer for stainless steel-based coated conductors,[13] whereas the latter conditions are considered to have high potential for coated conductor development from the view point of preventing Ni substrate oxidation.

Further texture assessment was carried out by XRD pole figure analysis (see Fig. 4). The (220) $CeO_2$ reflection was selected because it provides a clear separation from the YSZ peaks and gives a high intensity. From the pole figure of pure $CeO_2$ film [Fig. 4(a)], it can be scarcely detected there are four poles located at $\chi = 45°$, among a randomly oriented matrix. On the other hand, a typical pole figure of doped samples is shown in Fig. 4(b). It proves that grains develop a biaxial texture with a highly developed in-plane alignment, in agreement with RBS and RHEED measurements. The full width half-maximum (FWHM) of the (220) $\phi$-scan for these textured films is relatively constant at $1.2 \pm 0.1°$.

Thus, a clear scenario appears from our buffer layer morphological and structural analysis: Atomically flat and textured (001) ceria surfaces have been obtained. Theoretically, the $CeO_2$ (001) surface is unstable due to the polar nature of the fluorite crystal structure with alternating planes of oxygen and cerium ions.[36] Based on energetic criteria, the relative stability of the surfaces of $CeO_2$ is in the order (111) > (110) > (100).[37]

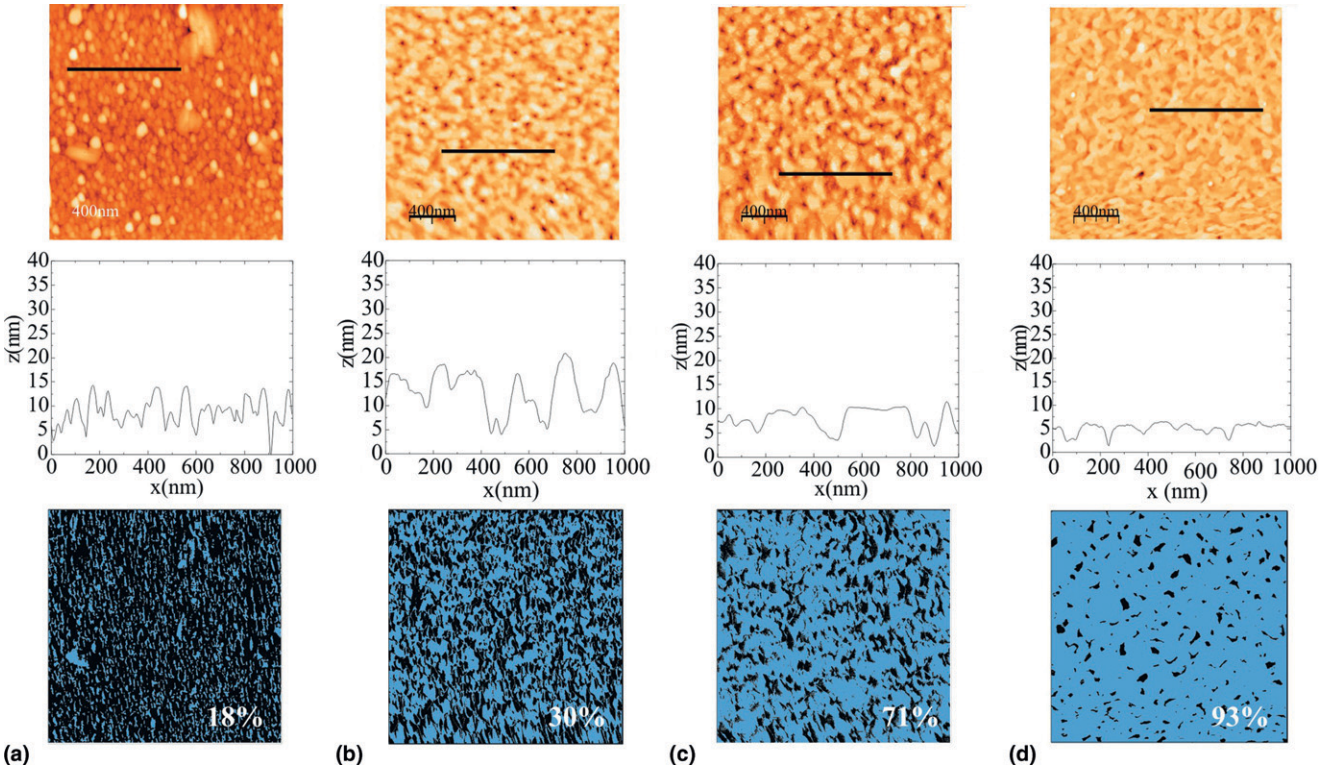


FIG. 2. AFM analysis (topographic images with the corresponding profile scan and binary image below) of (a) undoped $CeO_2$ in $Ar/H_2$, (b) CZO in $Ar/H_2$, (c) CGO in $Ar/H_2$, and (d) CZO in oxygen grown on YSZ at 900 °C for 8 h. The cross section is taken along the line in the AFM topographic image. (color online)

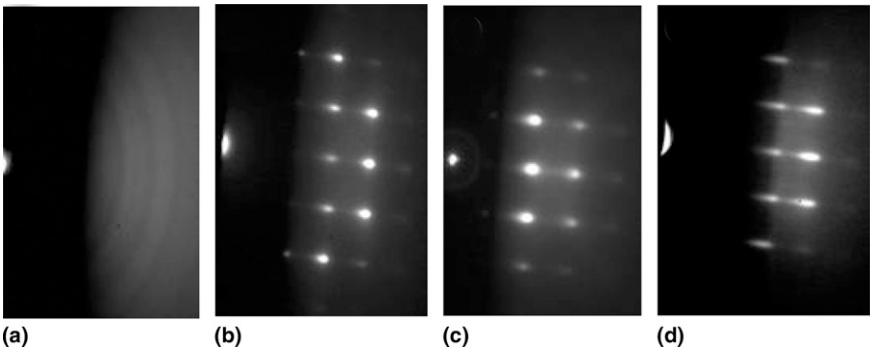


FIG. 3. RHEED pattern for a $CeO_2$-based cap layer on YSZ single crystal along the ⟨100⟩ of the substrate, (a) undoped $CeO_2$ grown in $Ar/H_2$ atmosphere, (b) CZO grown in $Ar/H_2$ atmosphere, (c) CGO grown in $Ar/H_2$ atmosphere, and (d) CZO in oxygen atmosphere.

A mechanism to stabilize a polar surface is by the reduction of surface charge. It might occur in several ways, including geometric reconstructions that force cations and anions to be in the same surface plane, an increase of oxygen vacancies, or possibly the exchange of oxygen at the surface. $Gd^{3+}$- and $Zr^{4+}$-doped $CeO_2$ samples are recognized as a reference formula for its high oxygen mobility because of the oxygen vacancies introduced for charge compensation.[38,39] Accordingly, it is not surprising that the incorporation of such dopants would be favorable to stabilize (001) surface. However, large and atomically flat terraces developed in oxygen processed films are attributed to different mechanism like some kind of surface reconstruction, which is now under study. In fact, the mechanism to stabilize the polar (001) $CeO_2$ surface is not yet fully established among experimentalists and more studies are needed.[17,40]

We note that simultaneously with the work reported in this article, we have carried out a detailed study focusing on the role of $Zr^{4+}$ and $Gd^{3+}$ on $CeO_2$ mobility.[19] We detected that both dopants increase mobility in MOD-$CeO_2$ lattice favoring the elimination of carbon impurities. As a result, $CeO_2$ films show a higher degree of

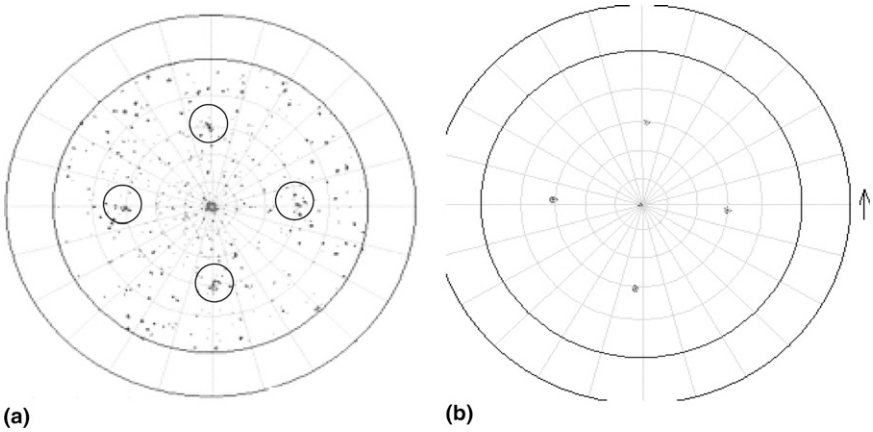


FIG. 4. XRD pole figure of (220) plane from (a) $CeO_2$ grown in $Ar/H_2$ atmosphere and (b) doped $CeO_2$ film grown on YSZ single-crystal substrate. Black circles in (a) show the four poles.

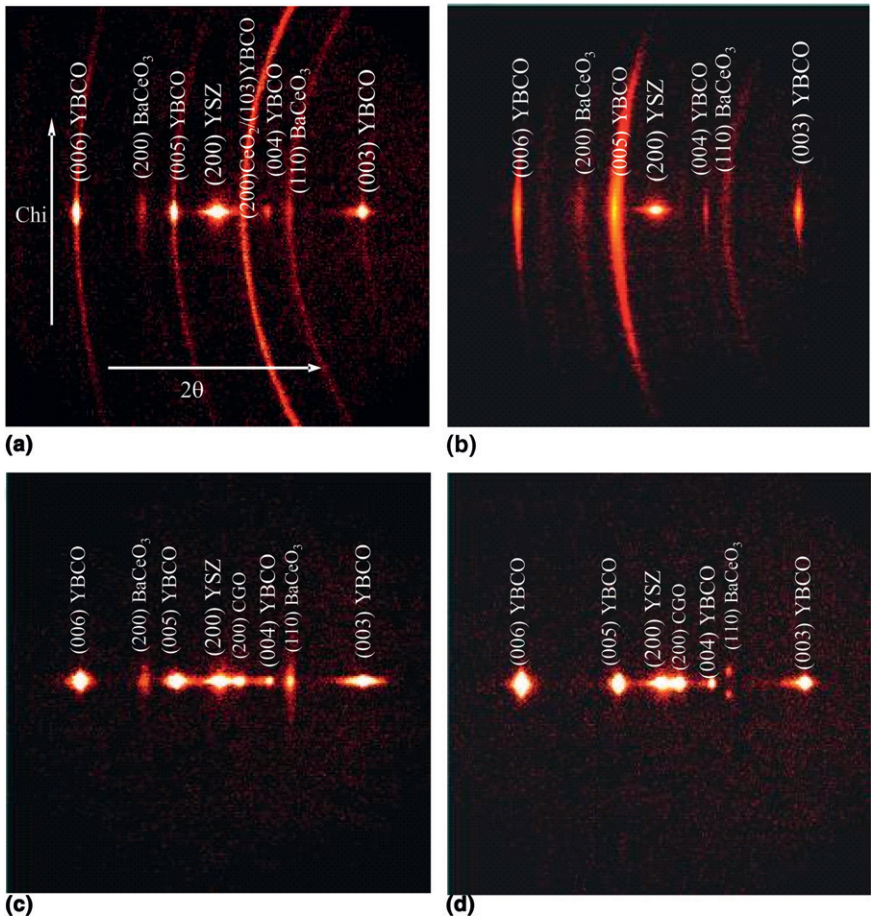


FIG. 5. XRD patterns of YBCO/$CeO_2$/YSZ multilayer films: θ–2θ Bragg–Brentano geometry where the Bragg peaks of the different phases are indicated. The $x$ axis corresponds to 2θ and the rings correspond to $\chi$, which varies with constant 2θ. (a) TFA-YBCO on MOD-$CeO_2$ films, (b) PLD-YBCO on MOD-$CeO_2$ films, (c) TFA-YBCO on MOD doped-$CeO_2$ films, and (d) PLD-YBCO on MOD doped-$CeO_2$ films. (color online)

epitaxy and a higher percentage of atomically flat area. However, it seems that a different mechanism is followed in each case. In the case of Gd–$CeO_2$, the increase of mobility is related to oxygen vacancies formation by charge compensation,[41] whereas for Zr-doped $CeO_2$ films, the key parameter appears to be the small ionic radius of $Zr^{4+}$.[42,43]

These differences in the surface quality of MOD-$CeO_2$ films have severe implications for the subsequent YBCO growth. To study how the $CeO_2$ surface

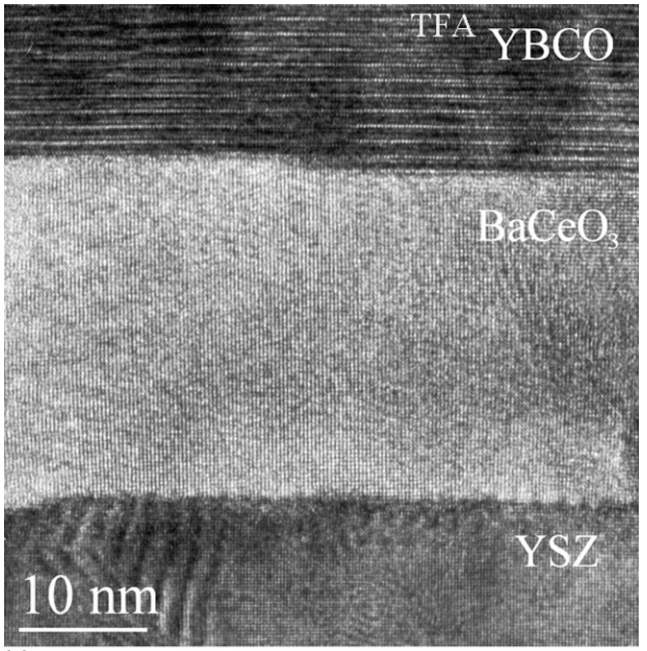


(a)

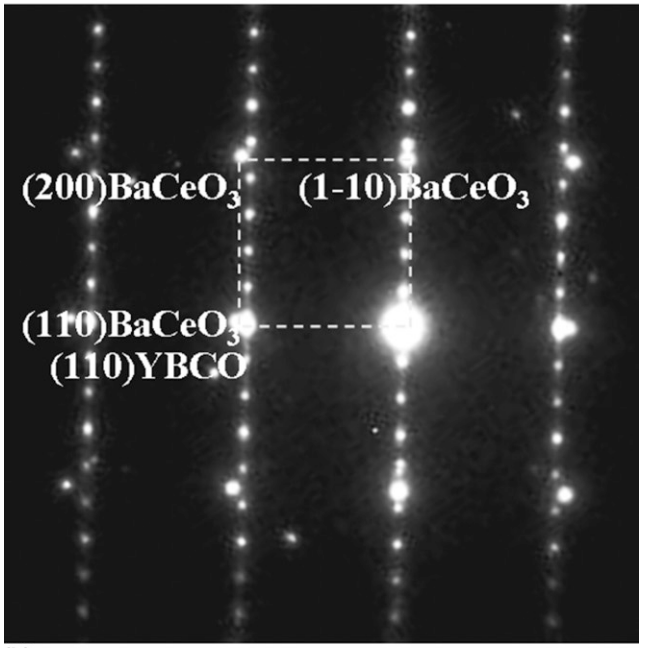


(b)

FIG. 6. (a) HRTEM image viewed along the ⟨110⟩ direction showing YBCO-$BaCeO_3$ interface. (b) SAD pattern showing the discrepancy of lattice parameters between YBCO and $BaCeO_3$.

morphology influences growth, YBCO films were grown on the as-described samples by two different routes: PLD and metalorganic decomposition using trifluoroacetates as precursors (TFA-MOD).

### B. YBCO films on MOD-$CeO_2$-based cap layers

The 200-nm TFA-YBCO and 300-nm PLD-YBCO layers were systematically grown on top of undoped and modified $CeO_2$ samples. The epitaxial quality and phase purity of YBCO films were examined by XRD analysis. We anticipated that no significant differences were observed in θ−2θ XRD diagrams for YBCO film on modified $CeO_2$ cap layers; therefore, for simplicity we compared θ−2θ XRD patterns of YBCO films grown on a pure $CeO_2$ cap layer with a representative θ−2θ XRD pattern of YBCO film on modified $CeO_2$ (see Fig. 5).

As a first step, we considered TFA and PLD layers on pure $CeO_2$ films shown in Figs. 5(a) and 5(b), respectively. Main peaks detected in these scans are (00*l*) from YBCO, (*h*00) from $CeO_2$, and (*h*00) from YSZ. We also identified (110) and (200) reflections from $BaCeO_3$ pseudocubic phase, which were also identified by TEM analysis. It is very important to emphasize that YBCO intensities are distributed in two contributions: discrete spots and ring structure suggesting a coexistence of epitaxial and randomly oriented phases, whereas intensities of $CeO_2$ and $BaCeO_3$ are distributed in a single ring structure indicating randomly oriented phases. Note that $BaCeO_3$ Bragg line reflections are slightly shifted from its reported 2θ values, this is because the incorporation of $Gd^{3+}$ (Gd:$BaCeO_3$) modifies the lattice parameter. By contrast, YBCO on modified $CeO_2$ films reveals isolated spots indicating a strong *c*-axis normal preferred orientation [TFA-YBCO in Fig. 5(c) and PLD-YBCO in Fig. 5(d)]. PLD-YBCO sample $BaCeO_3$ is detected as two discrete (110) peaks with only one orientation indicating that this perovskite structure, which has a high lattice misfit with YSZ, probably adopts a domain structure with[25] axes slightly deviating from perpendicularity respect to the substrate. These complex domain structures have been previously observed; for instance, in YBCO grown on YSZ when $BaZrO_3$ is formed as an intermediate reaction phase at the interface.[44] Interfacial reaction between YBCO and $CeO_2$ forming $BaCeO_3$ was previously reported by several groups.[45,46] We would like to note that from TEM analysis of all-chemical deposited films, i.e., TFA-YBCO/CGO/YSZ, we identified isolated areas where only YBCO and $BaCeO_3$ phases were observed (see Fig. 6). Figure 6(a) shows a cross-sectional HRTEM image viewed along the ⟨110⟩ YBCO direction. Well-textured YBCO film has been formed coinciding with the results observed in XRD data (Fig. 5). In addition, in this HRTEM image we can clearly observe that Gd:$BaCeO_3$ covers nearly the entire YSZ surface (∼30 nm thick), and the interface between YBCO and the film underneath is flat and free of precipitates or other reaction. These observations confirm the reaction between YBCO and $CeO_2$. Figure 6(b) shows a selected-area diffraction (SAD) pattern along the ⟨110⟩ YBCO direction taken in the vicinity of the interface of YBCO/$BaCeO_3$ of Fig. 6(a). The epitaxial relation between YBCO and $BaCeO_3$ is (1–10)$BaCeO_3$//(00l)YBCO and [110] $BaCeO_3$//[110]YBCO. The SAD pattern shows the

TABLE I. Summary of YBCO film texture measurements grown by PLD and TFA on MOD-ceria-based cap layer.

| Cap layer | Growth atmosphere | % atomically flat area | TFA-YBCO $\Delta\omega(005)$ (°) ±0.2 | TFA-YBCO $\Delta\phi(103)$ (°) ±0.2 | PLD-YBCO $\Delta\omega(005)$ (°) ±0.2 | PLD-YBCO $\Delta\phi(103)$ (°) ±0.2 |
|---|---|---|---|---|---|---|
| $CeO_2$ | $Ar/H_2$ | 18 | >5 | ... | >5 | ... |
| CZO | $Ar/H_2$ | 30 | 1.5 | 2.1 | 0.3 | 1.2 |
| CGO | $Ar/H_2$ | 71 | 0.5 | 1.2 | 0.3 | 1.2 |
| CZO | $O_2$ | 83 | 0.5 | 1.2 | 0.3 | 1.2 |

substantial mismatch ($\epsilon$ = 14%) between both layers, although YBCO film does not present distortion for $BaCeO_3$ formation. According to recent results concerning TFA-YBCO growth on substrates with different lattice misfits,[47] such large lattice mismatch between YBCO and $BaCeO_3$ leads to interfaces with high energies that would end in large YBCO dewetted areas. The nonobservance of any surface instability in our case reinforces a scenario where $BaCeO_3$ nucleates and grow after the epitaxial YBCO layers have already grown.[45,46]

Table I summarizes in-plane ($\phi$-scan) and out-of-plane ($\omega$-scan) texture determined for YBCO layers through (103) and (005) YBCO reflections, respectively. Better crystalline perfection for YBCO on modified $CeO_2$ samples is demonstrated by $\Delta\omega$ and $\Delta\phi$ values ($\Delta\omega \sim 0.3°$ and $\Delta\phi \sim 1.2°$ for PLD films and $\Delta\omega < 1.5°$ and $\Delta\phi < 2.1°$ for TFA films). These results correlate well with RHEED and RBS observations of $CeO_2$ films. Certainly, a highly biaxially textured YBCO film is obtained from highly crystalline-derived $CeO_2$ buffer layers. However, exploration of $J_c$ values will show that analysis of surface morphology buffer layer, in terms of atomically flat area, ultimately dictates YBCO film quality.

Figure 7(a) shows the dependence of $J_c$ values for all TFA-YBCO films on the percentage of atomically flat ceria-based buffer. We observe a gradual increase in $J_c$ values from 0–70% of flat area, beyond that value $J_c$ saturates carrying nearly 4 $MAcm^{-2}$ at 77K and self-field being the highest $J_c$ value reported to date for all chemical deposited $YBCO/CeO_2/YSZ$ multilayer systems. By contrast, PLD-YBCO films show a sharp increase in $J_c$ values from 18–30% of ceria flat area and then, the $J_c$ value achieves a constant value ~3.3 $MAcm^{-2}$ [see Fig. 7(b)]. Thus, these results confirm the significance of the control of the MOD-$CeO_2$ film flatness besides its epitaxial texture to obtain excellent TFA-YBCO film, and also suggest that CSD growth has some features that require an adequate process control. It is well known that nucleation of TFA-YBCO takes place exclusively at the interface with the substrate within a precursor,[48,49] showing anomalous large distances between nuclei.[50,51] During the growth process, these YBCO islands advance faster laterally and coalesce well before the nanocrystalline precursor is consumed. Our results suggest therefore that the atomically flat area of the cap layers behave as preferential nucleation centers,

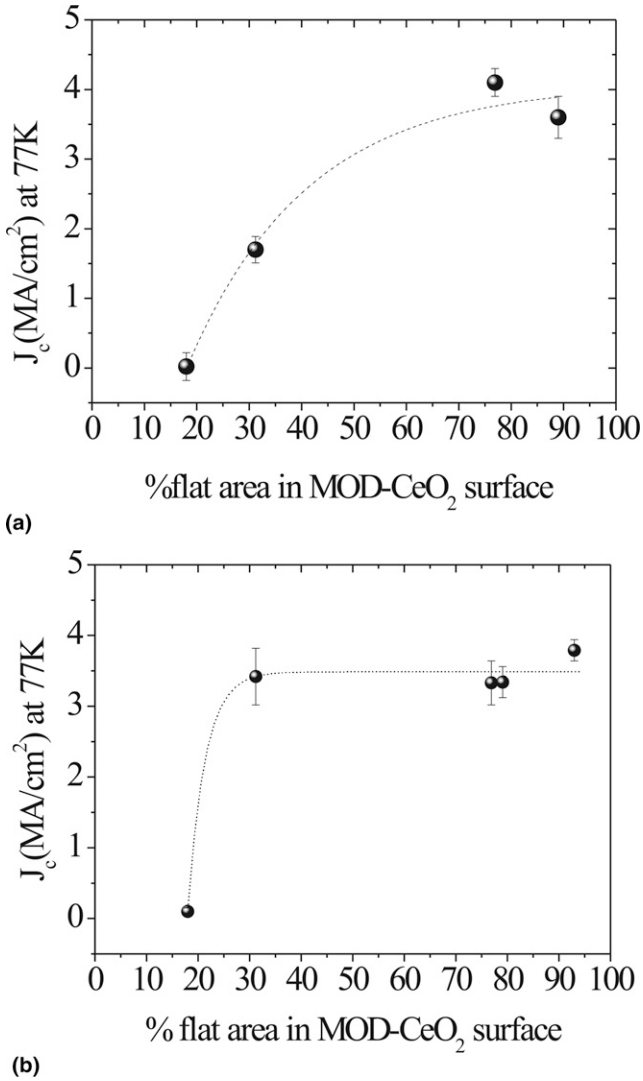


FIG. 7. Evolution of the critical current density at 77 K of (a) TFA-YBCO films and (b) PLD-YBCO films as a function of the percentage of ceria flatness. Line is a guide to the eyes.

i.e., they can have a catalytic effect on YBCO nucleation and growth, and when this area approaches ~70% TFA-YBCO films can grow preserving a highly epitaxial structure and avoid the formation of impurity phase at the grain boundaries.[52] If $CeO_2$ is rough with rounded grains, the density of nucleation centers is reduced and lateral growth of YBCO island is somehow hindered. Nonreacted nanocrystalline precursor may become

trapped at the grain boundaries or YBCO misoriented grains are formed, thus degrading in both cases the observed $J_c$ values. In the case of PLD-YBCO films, however, a slightly decreased influence on the cap layer flatness seems to occur and with $CeO_2$ cap layers having ~30% of atomic planarity the YBCO film already preserves a high epitaxial quality. The different influence of $CeO_2$ with PLD and TFA-YBCO films may be attributed to different YBCO nucleation rates, but a more detailed analysis would be required to clear up this point.

## IV. CONCLUSIONS

We have described an important advance in processing YBCO films on MOD- modified $CeO_2$ cap layers focusing on the interface quality between these layers. Critical current densities above 3 $MAcm^{-2}$ can be routinely achieved in both PLD and TFA-YBCO films deposited on MOD-$CeO_2$ cap layers.

We have shown that playing with dopant agents and processing atmosphere we can tune the quality of MOD-$CeO_2$ film. A fraction of polycrystalline ceria can be reduced to low values, especially for films grown under oxidizing atmosphere. In addition, this microstructural evolution goes along with an increase of the percentage of flatness stabilizing (001) ceria surface (>70% flatness versus 18%). These changes have been attributed to an increase of atom mobility, which enhances the epitaxial grain growth nucleated at the substrate interface. We proved that these changes in $CeO_2$ cap layer have direct implication in the growth and properties of TFA and PLD YBCO films. For the case of TFA-YBCO films, we have demonstrated that high crystalline $CeO_2$ film with an atomically flat (001) terraced surface are essential to obtain highly epitaxial YBCO films with high $J_c$ values: 4 $MAcm^{-2}$ at 77 K. Additionally, we identified the formation of Gd:$BaCeO_3$ phase as an interfacial product. Fully relaxed YBCO films and large lattice mismatch between YBCO/$BaCeO_3$ ($\epsilon$ ~14%) suggest interfacial reaction takes place after YBCO nucleation.

PLD-YBCO films revealed a less restrictive situation. Highly crystalline ceria with 30% of flat terraced surface is enough to obtain high quality YBCO films with $J_c$ values around 3 $MAcm^{-2}$ at 77 K. This is probably because the nucleation rate of YBCO is enhanced by a greater planarity of $CeO_2$. The different observed behavior of PLD and TFA YBCO films on MOD-$CeO_2$ cap layers can probably be attributed to a differing nucleation rate at the $CeO_2$ interface.

These are very important results because from this study emerged two potential cap layers to be transferred on metallic substrate: CGO grown in reducing atmosphere for Ni-RABiTs and oxygen processed ceria to IBAD-stainless steel.

## ACKNOWLEDGMENTS

We acknowledge the financial support from MEC (MAT2005-02047, and CONSOLIDER NANOSELECT), Generalitat de Catalunya (Catalan Pla de Recerca SGR-0029 and CeRMAE), EU (HIPERCHEM, NMP4-CT2005-516858). J. Gàzquez, M. Coll, and A. Pomar are grateful to Spanish Ministery of Educacion y Ciencia (MEC) for financial support through Formacion de Personal Investigador (FPI), Formacion de Profesorado Universitario (FPU), and "Ramón y Cajal" programs.

## REFERENCES

1. D.C. Larbalestier, A. Gurevich, D.M. Feldmann, and A. Polyanskii: High-$T_c$ superconducting materials for electric power applications. *Nature* **414,** 368 (2001).
2. M. Paranthaman and T. Izumi: High-performance YBCO-coated superconductor wires. *MRS Bull.* **29**(8), 533 (2004).
3. A. Usoskin and H.C. Freyhardt: YBCO-coated conductors manufactured by high-rate pulsed laser deposition. *MRS Bull.* **29,** 583 (2004).
4. P.N. Arendt and S.R. Foltyn: Biaxially textured IBAD-MgO templates for YBCO-coated conductors. *MRS Bull.* **29,** 543 (2004).
5. Y. Iijima, K. Kakimoto, Y. Yamada, T. Izumi, T. Saitoh, and Y. Shiohara: Research and development of biaxially textured IBAD-GZO templates for coated superconductors. *MRS Bull.* **29,** 564 (2004).
6. X. Obradors, T. Puig, A. Pomar, F. Sandiumenge, N. Mestres, M. Coll, A. Cavallaro, N. Roma, J. Gazquez, J.C. Gonzalez, O. Castano, J. Gutierrez, A. Palau, K. Zalamova, S. Morlens, A. Hassini, M. Gibert, S. Ricart, J.M. Moreto, S. Piñol, D. Isfort, and J. Bock: Progress towards all-chemical superconducting YBCO coated-conductors. *Supercond. Sci. Technol.* **19,** s1 (2006).
7. M.W. Rupich, D.T. Verebelyi, W. Zhang, T. Kodenkandath, and X. Li: Metalorganic deposition of YBCO films for second-generation high-temperature superconductor wires. *MRS Bull.* **29**(8), 572 (2004).
8. R.W. Schwartz, T. Schneller, and R. Waser: Chemical solution deposition of electronic oxide films. *Compt. Rendus Chem.* **7,** 433 (2004).
9. M.W. Rupich, W. Palm, W. Zhang, E. Siegal, S. Annavarapu, L. Fritzemeier, M.D. Teplitsky, C. Thieme, and M. Paranthaman: Growth and characterization of oxide buffer layers for YBCO coated conductors. *IEEE Trans. Appl. Supercond.* **9,** 1527 (1999).
10. Y.X. Zhou, X. Zhang, H. Fang, R.T. Putman, and K. Salama: Development of single solution buffer layers on textured Ni substrate for HTS coated conductors. *IEEE Trans. Appl. Supercond.* **15,** 2711 (2005).
11. M.P. Siegal, P.G. Clem, J.T. Dawley, R.J. Ong, M.A. Rodriguez, and D.L. Overmyer: All solution-chemistry approach for $YBa_2Cu_3O_{7-\delta}$-coated conductors. *Appl. Phys. Lett.* **80,** 2710 (2002).
12. S. Engel, K. Knoth, R. Hühne, L. Schultz, and B. Holzapfel: An all chemical solution deposition approach for the growth of highly textured $CeO_2$ cap layers on $La_2Zr_2O_7$-buffered long lengths of biaxially textured Ni–W substrates for YBCO-coated conductors. *Supercond. Sci. Technol.* **18,** 1385 (2005).
13. A. Pomar, A. Cavallaro, M. Coll, J. Gazquez, F. Sandiumenge, T. Puig, X. Obradors, and H.C. Freyhardt: All chemical YBaCuO-coated conductors on IBAD/YSZ substrates. *Supercond. Sci. Technol.* **19,** L1 (2006).
14. S. Sathyamurthy, M. Paranthaman, L. Heatherly, P.A. Martin, E.D. Specht, A. Goyal, T. Kodenkandath, X.P. Li, and M.W. Rupich: Solution-processed lanthanum zirconium oxide as a barrier layer for high I-c-coated conductors. *J. Mater. Res.* **21,** 910 (2006).

15. M.S. Bhuiyan, M. Paranthaman, S. Sathyamurthy, T. Aytug, S. Kang, D.F. Lee, A. Goyal, E.A. Payzant, and K. Salama: MOD approach for the growth of epitaxial $CeO_2$ buffer layers on biaxially textured Ni–W substrates for YBCO coated conductors. *Supercond. Sci. Technol.* **16,** 1305 (2003).
16. E. Stewart, M.S. Bhuiyan, S. Sathyamurthy, and M. Paranthaman: Studies of solution deposited cerium oxide thin films on textured Ni-alloy substrates for YBCO superconductor. *Mater. Res. Bull.* **41,** 1063 (2006).
17. A. Cavallaro, F. Sandiumenge, J. Gazquez, T. Puig, X. Obradors, J. Arbiol, and H.C. Freyhardt: Growth mechanism, microstructure and surface modification of nanostructured $CeO_2$ films by chemical solution deposition. *Adv. Funct. Mater.* **16,** 1363 (2006).
18. M. Coll, J. Gazquez, F. Sandiumenge, T. Puig, X. Obradors, J.P. Espinós, and R. Hühne: Nanostructural control in solution-derived epitaxial $Ce_{1-x}Gd_xO_{2-y}$ films. *Nanotechnology* **19,** 395601 (2008).
19. M. Coll, J. Gazquez, C. Mansilla, J. Espinos, Y. Morrilla, J. Garcia, F. Sandiumenge, T. Puig, and X. Obradors: (in preparation).
20. D.E. Wesolowksi and M.J. Cima: Nitrate-based metalorganic deposition of $CeO_2$ on yttria-stabilized zirconia. *J. Mater. Res.* **21,** 1 (2006).
21. K. Develos-Bagarinao, H. Yamasaki, and Y. Nakagawa: Effect of surface modification of $CeO_2$ buffer layers on $J_c$ and defect microstructures of large-area YBCO thin films. *Supercond. Sci. Technol.* **19,** 873 (2006).
22. A. Hassini, A. Pomar, J. Gutiérrez, M. Coll, N. Romà, C. Moreno, A. Ruyter, T. Puig, and X. Obradors: Atomically flat MOD $La_{0.7}Sr_{0.3}MnO_3$ buffer layers for high critical current $YBa_2Cu_3O_7$ TFA films. *Supercond. Sci. Technol.* **20,** S230 (2007).
23. A. Pomar, M. Coll, A. Cavallaro, J. Gazquez, N. Mestres, F. Sandiumenge, T. Puig, and X. Obradors: Interface control in all metallorganic deposited coated conductors: Influence on critical currents. *J. Mater. Res.* **21,** 2176 (2006).
24. M. Coll, A. Pomar, T. Puig, and X. Obradors: Atomically flat surface: The key issue for solution-derived epitaxial multilayers. *Appl. Phys. Exp.* **1,** 121701 (2008).
25. A. Pomar, M. Coll, A. Cavallaro, J. Gazquez, J.C. Gonzalez, N. Mestres, F. Sandiumenge, T. Puig, and X. Obradors: All-chemical high-$J_c$ $YBa_2Cu_3O_7$ multilayers with $SrTiO_3$ as cap layer. *J. Mater. Res.* **21,** 1106 (2006).
26. N. Romà, S. Morlens, S. Ricart, K. Zalamova, J.M. Moreto, A. Pomar, T. Puig, and X. Obradors: Acid anhydrides: A simple route to highly pure organometallic solutions for superconducting films. *Supercond. Sci. Technol.* **19,** 521 (2006).
27. K. Zalamova, N. Romà, A. Pomar, S. Morlens, T. Puig, J. Gázquez, A.E. Carrillo, F. Sandiumenge, S. Ricart, N. Mestres, and X. Obradors: Smooth stress relief of trifluoroacetate metal-organic solutions for $YBa_2Cu_3O_7$ film growth. *Chem. Mater.* **18,** 5897 (2006).
28. T. Puig, J.C. Gonzalez, A. Pomar, N. Mestres, O. Castano, M. Coll, J. Gazquez, F. Sandiumenge, S. Piñol, and X. Obradors: Influence of growth conditions on the microstructure and critical currents of TFA-MOD $YBa_2Cu_3O_7$ films. *Supercond. Sci. Technol.* **18,** 1141 (2005).
29. R. Hühne, D. Selbmann, J. Eickemeyer, J. Hanisch, and B. Holzapfel: Preparation of buffer layer architectures for $YBa_2Cu_3O_{7-x}$ coated conductors based on surface oxidized Ni tapes. *Supercond. Sci. Technol.* **19,** 169 (2006).
30. L.C. Feldman, J.W. Mayer, and S.T. Picraux: *Materials Analysis by Ion Channeling* (Academic Press, New York, 1982).
31. I. Horcas, R. Fernández, J.M. Gómez-Rodríguez, and J. Colchero: WSxM: A software for scanning-probe microscopy and a tool for nanotechnology. *Rev. Sci. Instrum.* **78,** 013705 (2007).
32. R.L. Flemming: Micro x-ray diffraction (μXRD): A versatile technique for characterization of earth and planetary materials. *Can. J. Earth Sci.* **44,** 1333 (2007).
33. B.B. He: Introduction to two-dimensional x-ray diffraction. *Powder Diffr.* **18,** 71 (2003).
34. A. Sanchez and C. Navau: Magnetic properties of finite superconducting cylinders. I. Uniform applied field. *Phys. Rev. B* **64,** 214507 (2001).
35. M. Coll, J. Gazquez, T. Puig, and X. Obradors: (in preparation).
36. C. Noguera: Polar oxide surfaces. *J. Phys.: Condens. Matter* **12,** R367 (2000).
37. T.X.T. Sayle, S.C. Parker, and C.R.A. Catlow: The role of oxygen vacancies on ceria surfaces in the oxidation of carbon-monoxide. *Surf. Sci.* **316,** 329 (1994).
38. G. Balducci, M. Islam, J. Kaspar, P. Fornasiero, and M. Graziani: Bulk reduction and oxygen migration in the ceria-based oxides. *Chem. Mater.* **12,** 677 (2000).
39. T.H. Etsell and S.N. Flengas: Electrical properties of solid oxide electrolytes. *Chem. Rev.* **70,** 339 (1970).
40. S.N. Jacobsen, U. Helmersson, R. Erlandsson, B. Skarman, and L.R. Wallenberg: Sharp microfaceting of (001)-oriented cerium dioxide thin films and the effect of annealing on surface morphology. *Surf. Sci.* **429,** 22 (1999).
41. P.L. Chen and I.W. Chen: Grain growth in $CeO_2$: Dopant effects, defect mechanism, and solute drag. *J. Am. Ceram. Soc.* **79,** 1793 (1996).
42. G. Balducci, J. Kaspar, P. Fornasiero, M. Graziani, M. Saiful Islam, and J.D. Gale: Computer simulation studies of bulk reduction and oxygen migration in $CeO_2$–$ZrO_2$ solid solutions. *J. Phys. Chem. B* **101,** 1750 (1997).
43. E. Mamontov, T. Egami, R. Brezny, M. Koranne, and S. Tyagi: Lattice deffects and oxygen storage capacity of nanocrystalline ceria and ceria-zirconia. *J. Phys. Chem. B* **104,** 11110 (2000).
44. D.C. Schlom, E.S. Hellman, E.H. Hartford, C.B. Eom, J.C. Clarck, and J. Mannhart: Origin of the $\varnothing \sim \pm 9°$ peaks in $YBa_2Cu_3O_{7-\delta}$ films grown on cubic zirconia substrates. *J. Mater. Res.* **11,** 1336 (1996).
45. J.S. Matsuda, T. Tokunaga, K. Nakaoka, R. Teranishi, Y. Aoki, H. Fuji, A. Yajima, Y. Yamada, T. Izumi, and Y. Shiohara: Transmission electron microscopic studies on crystallization of YBCO films deposited by advanced TFA-MOD method. *Physica C* **426,** 1051 (2005).
46. D.E. Wesolowski and M.J. Cima: Large area quantification of $BaCeO_3$ formation during processing of metalorganic-deposition-derived YBCO films. *J. Mater. Res.* **22,** 1077 (2007).
47. M. Coll, J. Gazquez, A. Pomar, T. Puig, F. Sandiumenge, and X. Obradors: Stress-induced spontaneous dewetting of heteroepitaxial $YBa_2Cu_3O_7$ thin films. *Phys. Rev. B* **73,** 075420 (2006).
48. P.C. McIntyre and M.J. Cima: Heteroepitaxial growth of chemically derived ex-situ $Ba_2YCu_3$ $O_{7-x}$ thin films. *J. Mater. Res.* **9,** 2219 (1994).
49. L. Wu, Y. Zhu, V.F. Solovyov, H.J. Wiesmann, A. R. Moodenbaugh, R.L. Sabatini, and M. Suenaga: Nucleation and growth of $YBa_2Cu_3O_x$ on $SrTiO_3$ and $CeO_2$ by a $BaF_2$ post-deposition reaction process. *J. Mater. Res.* **16,** 2869 (2001).
50. J. Gazquez, F. Sandiumenge, M. Coll, A. Pomar, N. Mestres, T. Puig, X. Obradors, Y. Kihn, M.J. Casanove, and C. Ballesters: Precursor evolution and nucleation mechanism of $YBa_2Cu_3O_x$ films by TFA metal-organic decomposition. *Chem. Mater.* **18,** 6211 (2006).
51. V.F. Solovyov, H.J. Wiesmann, and M. Suenaga: Nucleation of YBCO on buffered metallic substrates in thick precursor films made by the $BaF_2$ process. *Supercond. Sci. Technol.* **18,** 239 (2005).
52. S. Solovyov, Q. Li, H. Wiesmann, P. Oleynikov, and Y. Zhu: Strong influence of the $YBa_2Cu_3O_7$ grain size on critical current densities of thick $YBa_2Cu_3O_7$ layers made by a metal–organic deposition process. *Supercond. Sci. Technol.* **21,** 125013 (2008).